

[PT]

Quantitative approach to physical and chemical gold mobility in equatorial rainforest lateritic environment

F. Colin ^a, P. Vieillard ^b and J.P. Ambrosi ^c

^a ORSTOM, UM GECO, Laboratoire de Géosciences de l'Environnement, Université Aix-Marseille III, 13397 Marseille Cédex 13, France

^b Laboratoire de Pétrologie de la Surface, U.A. CNRS 721, Université de Poitiers, 40 avenue du Recteur Pineau, 86022 Poitiers Cédex, France

^c Laboratoire de Géosciences de l'Environnement, URA CNRS 132, Université Aix-Marseille III, 13397 Marseille Cédex 13, France

Received April 15, 1992; revision accepted October 26, 1992

ABSTRACT

Mobility of gold throughout the global weathering system of Dondo Mobi, South Gabon, has been quantitatively addressed by calculating the gold mass transfer during lateritic weathering of auriferous lisvenite, Archean gneiss and Proterozoic schist, and by proposing a thermodynamic approach to gold solubility under equatorial rainforest acidic conditions.

Both chemical and short-distance translocation processes govern the mobility of gold and gold particles during the long-term evolution of collapsed open weathering systems, which result from the combined interaction of rock, meteoric water and biological agents. Free gold particles are translocated from the lisvenite-derived soil towards formerly barren Archean gneiss and porous Proterozoic formations derived from schist, to form a 200 m wide supergene gold dispersion halo, which took shape over about 0.86–1.26 million years.

Simultaneously with physical translocation of gold, dissolution of gold makes the total balance of gold transfer through the whole weathering system strongly negative, which is the converse of what is generally believed to occur in lateritic systems. Taking into account hydrolysis reactions, three main gold complexes are proposed as a function of corresponding inorganic and organic ligand concentrations. These are: $\text{Au}(\text{OH})_3(\text{H}_2\text{O})^0$, AuClOH^- and $\text{Au}(\text{OH})_2\text{FA}^-$. These gold complexes leave the Dondo Mobi weathering mantle and move towards the river system in the course of both physical and chemical processes involved in the weathering of the formation.

1. Introduction

Gold exploration as an economic priority in tropical or sub-tropical countries [1–3] has indirectly accelerated efforts to understand the behaviour of gold within surficial lateritic formations.

The chemical mobility of gold has been inferred from a qualitative point of view by determining surface dispersion patterns [2–4] and by identifying the morphology and the chemical composition of both residual and supergene gold

grains [2,5–12]. A thermodynamic approach was used and it was assumed that experimental results of gold dissolution [13–19] were applicable to natural, open systems. Within weathering mantles derived from sulphide–carbonate-bearing protore, the supergene chemical mobility is controlled by the stability of thiosulphate complexes ($\text{Au}(\text{S}_2\text{O}_3)_2^{3-}$) during mildly acid to slightly alkaline oxidative weathering, and of bisulphide complexes ($\text{Au}(\text{HS})_2^-$) in more reducing conditions [2,9,12,19,20]. In the absence of significant concentrations of such ligands, gold complexes in lateritic formations are believed to be dominated by auric chloride (AuCl_4^-) [2,3,9], which is stable only in very acidic, highly oxidizing and chloride-rich media. Such models, however, cannot be applied to most of the surficial lateritic porous

Correspondence to: F. Colin, ORSTOM, UM GECO, Laboratoire de Géosciences de l'Environnement, Université Aix-Marseille III, 13397 Marseille Cédex 13, France.



media, which are drained by slightly to moderately acid and very diluted waters [11,21].

The reason for the physical mobility of gold grains has been stated as being due to a number of causes: from in situ gravitational settling [2,8,9]; as a consequence of termite activity [22]; indirectly induction by gold-bearing pisolite dispersion [23]; or as a probable result of surface washing during regolith reduction [2].

The difficulty in localizing the mineralized source protore, the heterogeneity in gold content distribution, the discrepancy between experimental and natural systems, the lack of mass balance relationships based on petrological data of gold host weathered rocks, and the complex history of the polygenic lateritic systems [24], are the reasons why there are considerable uncertainties about quantification of physical and chemical supergene gold mobility, transport distances, and enrichment or depletion rates in surficial weathering systems under lateritic conditions.

The gold dispersion halo developed at Dondo Mobe (11°35'E, 1°17'S) under equatorial humid rainforest conditions (mean annual rainfall around 2000 mm), has recently been qualitatively studied [11]. The halo forms from the weathering of auriferous lisvenite and spreads laterally within Proterozoic schist and surface layers derived from Archean gneiss (Fig. 1). Within the lower saprolite, gold (which is visible to the naked eye) is closely associated with its auriferous parent rock. From a petrological study of host rocks and gold particles themselves, it has been demonstrated that the surficial, dispersed visible gold consists of residual gold particles inherited from the lisvenite source, and that such gold particles are, in addition, clearly affected by dissolution processes [11].

The aim of this paper is to determine quantitatively the physical and chemical mobility of all the gold within the weathering system of Dondo Mobe by calculating the gold mass transfer during

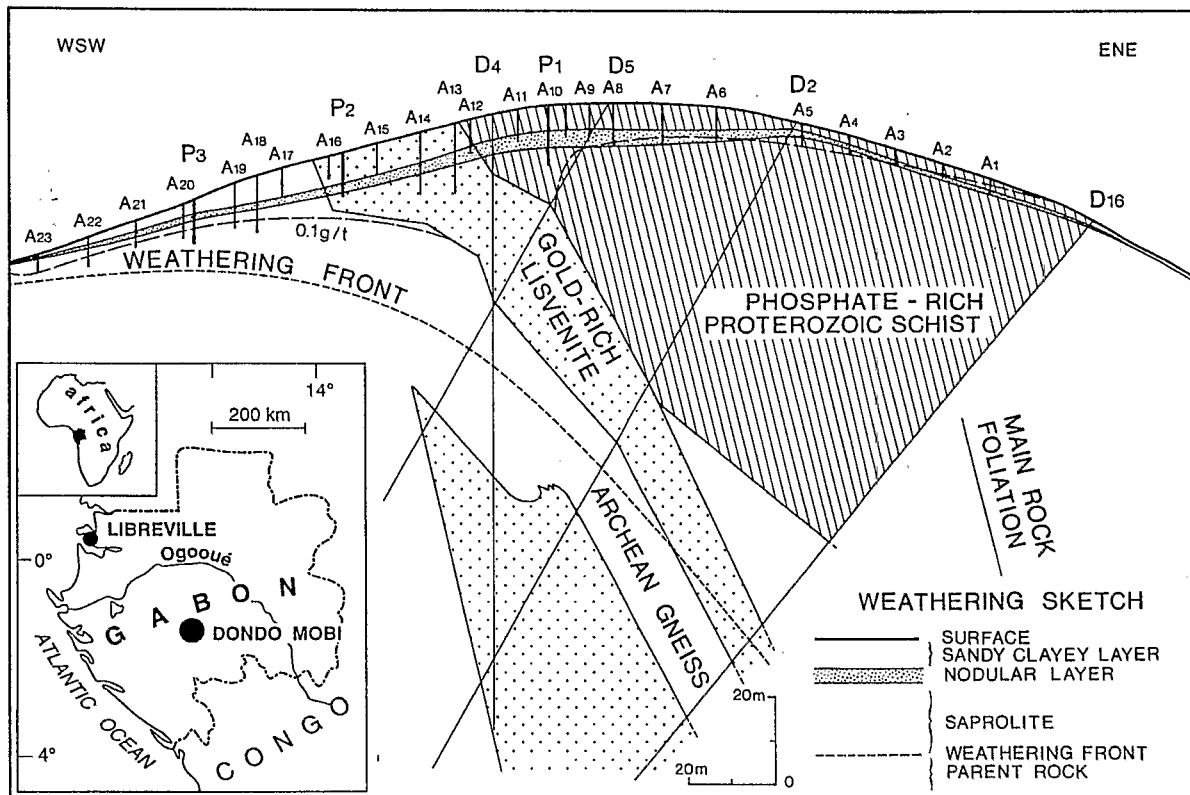


Fig. 1. Geographic setting of the Dondo Mobe gold deposit and cross section of the Dondo Mobe weathering mantle showing the location of pits (P), diamond drill holes (D) and auger holes (A) used in this study.

weathering and by proposing a new thermodynamic approach to gold solubility under equatorial rainforest conditions.

2. Sampling and experimental methods

The samples of fresh and weathered rocks (3 kg) were collected from drill core holes, auger holes and pits throughout the deposit (Fig. 1) after macroscopic description in the field. Samples from drill core holes and pits (carefully gathered with preserved texture) were used for chemical analyses, mineral determinations and density (bulk and grain) measurements. Samples from auger holes were only analyzed for gold content determination and the results are reported in [3,11]. Concerning chemical analyses in the laboratory, the samples were dried at 60°C and completely dissolved by tri-acid attack. Gold was extracted from solution using MIBK (methylisobutylketone) and measured by atomic absorption spectrophotometry (lower detection limit = 1 ppb, uncertainty = 5%). Major and trace element contents were determined by inductive coupled plasma spectroscopy (ICP).

Bulk density (ρ_w) measurements were made on rock samples after drying by weighting and coating them with molten paraffin wax, followed by immersion in water to measure their displaced volume. Bulk density was estimated by mass per unit volume with errors of about 1%. Grain density (ρ_g) was measured by air pycnometer with errors of about 1%. Porosity (ϕ) was calculated from the equation $\phi = 1 - \rho_w/\rho_g$.

Spring waters were collected around the deposit and titrated with AgNO_3 with $\pm 1\%$ accuracy to determine the chlorine content. The pH of the soil and spring water were measured with an accuracy of ± 0.1 pH using a glass electrode (U-7 Horiba water checker).

According to [25] and [26], the average concentration of soluble humic substances has been fixed at 5 mg/l in our surficial weathering system. The O_2 fugacity was fixed for all thermodynamic calculations at $f_{\text{O}_2} = 10^{-0.68}$, which corresponds to the atmospheric value. We choose that value to simulate the behaviour of gold under oxidative conditions, for example, an Eh value ranging from 983 mV at pH 4 to 861 mV at pH 6, which we believed appropriate to very surficial and well ventilated lateritic systems [24], as well as to

equatorial rainforest river systems [21]. The possible f_{O_2} changes in weathering solutions will be not investigated here.

The interpretation of metal mobility in weathering systems requires rigorous means of calculating losses or gains in relation to parent rock. The first mass balance calculations were based on iso-element changes during the conversion of fresh rocks to weathered materials [27,28]. Iso-volumetric mass balance calculations were applied for the first time in 1955, for the determination of mass transfers in saprolite [29]. Since that time, numerous workers have carried out mass balance calculations to determine transfers during weathering, and formal mass balance principles were presented as functional forms of constitutive relationships between the chemical composition of weathered material, its bulk density, porosity and volume change, in relation to corresponding chemical and physical properties of fresh parent rocks [30]. These equations (eqs. (1-3)), where subscripts w and p refer to the physical and chemical properties of weathered and parent rock, respectively, are used in our work. Thus, volumetric change is defined by:

$$\epsilon_{i,w} = \frac{\rho_p C_{i,p}}{\rho_w C_{i,w}} - 1 \quad (1)$$

where: i = an element considered as immobile during weathering; ρ = the bulk density (in g/cm^3); c = the concentration (in $\text{g}/100 \text{ g}$).

Extraction or addition of a chemically mobile element, j , either by solute migration or physical translocation is quantified by the open-system mass transport function ($\tau_{j,w}$) defined by:

$$\tau_{j,w} = 100 \frac{m_j}{c_{j,p} \rho_p V_p} \quad (2)$$

$\tau_{j,w}$ reflects a true mass gain in element j (m_j in grams) in the weathered rock compared to the parent rock volume (V_p in cubic centimetres), while a negative value indicates a mass loss.

The enrichment factor (the ratio of the concentrations of an element j in the weathered material to that of the fresh parent rock) is clearly defined as being dependant upon residual enrichment, volumetric change and the gain or loss in mass:

$$\frac{c_{j,w}}{c_{j,p}} = \frac{\rho_p}{\rho_w} \frac{1}{\epsilon_{i,w} + 1} (1 + \tau_{j,w}) \quad (3)$$

In order to calculate both the volumetric changes and net gains or losses of any element, it is necessary to identify an element that is immobile in the physical and chemical paths of the weathering system studied. Petrological studies [31] showed that zirconium was a suitable element for use in our study. This zirconium is present in the autochthonous zircons in the parent rocks from which the weathered materials were derived. Hence i will be replaced by Zr in the following equations.

3. Results and discussion

3.1 Weathering patterns

The global weathering system of Dondo Mobi can be divided into three sub-systems, depending on their referral parent rock. The depth of leach-

ing locally reaches thicknesses of up to 100 m. Each sub-system consists of three main weathering layers, which are (from the fresh rock to the surface): the saprolite, the nodular layer and the sandy-clayey layer (Fig. 1). The auriferous lisvenite formation and the layers derived from it by weathering are located in the central part of the weathering mantle, whereas the Proterozoic weathered schist extends up-slope, in the east-northeast direction, and fresh plus weathered Archean gneiss spreads down-slope in the west-southwest direction. A 0.1 m thick organic layer covers the sandy-clayey layer. The thickness of the saprolite (given by the weathering front course) increases towards the east-northeast. The results of mineralogical composition, bulk density, porosity, volumetric change, gold content and calculation of net mass gain/loss (transport function) of gold for samples from each layer are

TABLE 1

Physical and chemical data for fresh lisvenite and derived weathering rocks

sample location	layer	main phases	depth (m)	ρ (gcm ⁻³)	ϕ	$\epsilon_{Zr,w}$	Au (ppm)	$\tau_{Au,w}$
P2	s.c.	Q-K	0.50	1.59	0.37	-0.64	3.279	-0.85
P2	s.c.	Q-K	3.50	1.36	0.45	-0.71	1.934	-0.94
P2	s.c.	Q-K	5.50	1.51	0.43	-0.78	4.209	-0.90
P2	n.	G	7.20	1.79	0.33	-0.73	0.550	-0.98
P2	n.	Q-G	7.60	1.99	0.24	-0.74	0.316	-0.99
P2	sap.	Q-K	8.20	2.20	0.15	-0.88	6.310	-0.87
D2	sap.	Q-K	58.40	1.85	0.31	-0.56	24.500	+0.63
D2	sap.	Q-K	59.32	1.31	0.51	-0.14	0.650	-0.94
D2	sap.	S-K	60.19	1.27	0.52	-0.44	0.180	-0.99
D2	sap.	S-K	61.92	1.40	0.46	-0.75	19.900	-0.43
D2	sap.	S-K	62.00	1.30	0.52	-0.63	2.000	-0.92
D2	sap.	S-K	62.85	1.50	0.45	-0.77	3.300	-0.91
D2	sap.	S-K	62.90	1.59	0.42	-0.45	70.000	+3.98
D2	sap.	Q-K	63.22	1.52	0.39	+0.02	1.200	-0.85
D2	sap.	S-K	64.08	1.52	0.40	-0.52	1.800	-0.89
D2	sap.	C	65.00	1.77	0.32	+0.82	0.001	-1.00
D2	p.*	A-C-Q-CH	83-117	2.69	0.03	0	4.576	0
D4	sap.	Q	14.50	1.92	0.36	-0.77	1.500	-0.95
D4	sap.	K-Q	16.00	1.33	0.51	-0.71	6.200	-0.80
D4	sap.	K-Q	20.00	1.40	0.50	-0.81	0.990	-0.98
D4	sap.	K-Q	22.00	1.40	0.50	-0.65	0.580	-0.98
D4	sap.	K-Q	33.00	1.27	0.51	-0.67	1.900	-0.93
D5	sap.	K-Q	25.63	1.65	0.39	-0.77	0.545	-0.98
D4	sap.	K-Q	30.74	1.52	0.38	-0.33	0.300	-0.97
D4	sap.	S-K	39.00	1.44	0.44	-0.77	0.615	-0.98
D4	sap.	Q-K	40.00	1.46	0.42	-0.45	0.455	-0.97
D16	sap.	CH-V	85.71	1.65	0.31	-0.58	0.320	-0.98
D16	sap.	CH-V	86.56	1.93	0.21	-0.54	5.700	-0.59
D16	sap.	CH-V	87.50	2.48	0.07	-0.68	0.100	-0.99

P = pit; D = diamond drill hole; s.c. = sandy-clayey; n. = nodular; sap. = saprolite; p.* = 23 parent rocks (Au ranging from 0.020 to 81 ppm); Q = quartz; K = kaolinite; G = goethite; S = smectite; A = amphibole; C = carbonate; CH = chlorite; V = vermiculite; ρ = bulk density; ϕ = porosity; $\epsilon_{Zr,w}$ = volumetric change; $\tau_{Au,w}$ = transport function.

given in Table 1 for the lisvenite system, in Table 2 for the Archean gneiss system and in Table 3 for the Proterozoic schist system.

The primary gold mineralization occurs in quartz veins which cross-cut the lisvenite (Fig. 1). The lisvenite consists mainly of assemblages of quartz, carbonate, amphibole and chlorite. The main components of the fresh Archean gneiss are quartz and mica, with minor feldspar and chlorite and the Proterozoic schist consists mainly of quartz and mica and accessory graphite. Weathering leads to saprolite formation, by replacement of primary minerals by smectite and kaolinite (apart from quartz and muscovite there is only partial weathering). The overlying nodular layer, in which the parent rock texture is obliterated, consists of a quartz-kaolinite bearing matrix with numerous, scattered goethite-rich, kaolinite-rich and gibbsite-rich nodules. These are interpreted as being relic and/or degradation stages of ancient iron crust formation [32]. The upper layer (i.e., the sandy clayey layer) exhibits a fine micro-aggregated quartz-kaolinite-rich matrix, characterized by pedoturbation features, which are due to biological and geochemical processes. Physically, the weathering of parent rocks is, in general, manifested by an upwards increase in porosity (correlated to bulk density decrease) and in increase in negative volumetric changes (collapse); except in the very surficial part of the

sandy-clayey layer, where collapse is reduced due to root activity.

3.2 Gold enrichment factor and transport function variation field

Rewriting eq. (3), with gold as the mobile element, j , gives eq. (4), which defines the ratio "gain or loss" versus volumetric change as a function of the product of the density ratio times the enrichment factor, a term which is also the volumetric concentration ratio of gold ($R_{w/p}$):

$$\frac{\tau_{Au,w} + 1}{\epsilon_{Zr,w} + 1} = \frac{\rho_w}{\rho_p} \frac{c_{Au,w}}{c_{Au,p}} = R_{w/p} \quad (4)$$

It is then possible to study the variation of $\tau_{Au,w}$ (transport function) as a function of $R_{w/p}$ (volumetric concentration ratio) and of $\epsilon_{Zr,w}$ (volumetric change). The results are shown in Fig. 2.

Volumetric change is equal to 0 when the change in bulk density is exactly inversely proportional to the change in zirconium concentration in the weathering system with respect to the corresponding parent rock. The transformation is then iso-volumetric. When the product bulk density times zirconium concentration in the weathered system is greater than the same product for parent rock, the volumetric change is negative. The transformation is then associated with col-

TABLE 2

Physical and chemical data for fresh gneiss and derived weathering rocks

sample location	layer	main phases	depth (m)	ρ (gcm ⁻³)	ϕ	$\epsilon_{Zr,w}$	Au (ppm)	$\tau_{Au,w}$
P3	s.c.	Q-K	0.50	1.57	0.41	-0.19	0.633	+300.67
P3	s.c.	Q-K	1.50	1.59	0.40	-0.06	0.506	+282.89
P3	s.c.	Q-K	2.70	1.50	0.42	-0.27	0.380	+156.57
P3	n.	Q-K	3.20	1.59	0.41	-0.25	0.327	+145.77
P3	sap.	Q-G	3.60	1.67	0.37	-0.45	0.237	+80.50
P3	sap.	Q-G	4.20	1.71	0.34	-0.33	0.045	+18.30
P3	sap.	Q-G	5.50	1.74	0.32	-0.26	0.019	+8.19
D2	sap.	Q-K	71.00	2.60	0.04	+0.06	0.001	+0.04
D4	sap.	Q-K	50.00	2.30	0.17	-0.34	0.001	-0.43
D4	sap.	Q-K	53.00	2.50	0.09	-0.37	0.001	-0.40
D4	sap.	Q-M	54.00	2.71	0.02	-0.38	0.001	-0.37
D5	sap.	Q-K	44.00	1.85	0.30	+0.23	0.001	-0.14
D2,4,5	p.*	Q-M	52-135	2.65	0.02	0	0.001	0

P = pit; D = diamond drill hole; s.c. = sandy-clayey; n. = nodular; sap. = saprolite; p.* = 9 parent rocks; Q = quartz; K = kaolinite; G = goethite; M = mica; ρ = bulk density; ϕ = porosity; $\epsilon_{Zr,w}$ = volumetric change, $\tau_{Au,w}$ = transport function.

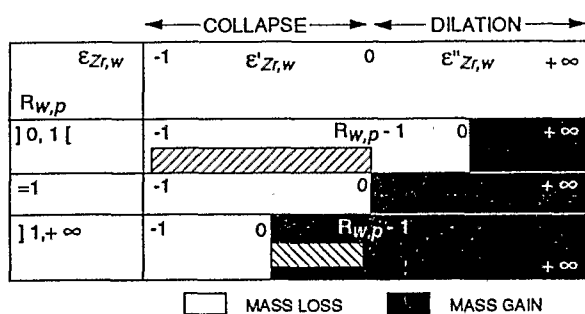


Fig. 2. Variation in the gold transport function $\tau_{Au,w}$ versus volumetric change ($\epsilon_{Zr,w}$) and concentration ratio $R_{w,p}$. Hatching from left to right = lisenite sub-system; hatching from right to left = the gneiss plus schist sub-systems.

lapse, which ranges in theory from 0^- to -1 . Inversely, the volumetric change is positive and the transformation is dilational, with a range of dilation from 0^+ to $+\infty$. The volumetric changes given in Tables 1–3 average negative values for each layer of the three sub-systems. The weathered lisenite formation is collapsed by 0.68 in the saprolite, by 0.74 in the nodular layer and by 0.71 in the sandy-clayey layer. The formation derived from gneiss is collapsed by 0.17 in the saprolite, by 0.35 in the nodular layer and by 0.17 in the sandy-clayey layer. The weathered schist is collapsed by 0.34 in the saprolite, by 0.69 in the nodular layer and by 0.60 in the sandy-clayey

TABLE 3

Physical and chemical data for schist derived weathering rocks

sample location	layer	main phases	depth (m)	ρ (gcm ⁻³)	ϕ	$\epsilon_{Zr,w}$	Au (ppm)	$\tau_{Au,w}$
P1	s.c.	QK	0.50	1.48	0.40	-0.73	1.300	+356.56
P1	s.c.	QK	2.50	1.58	0.42	-0.70	2.930	+939.99
P1	s.c.	QK	4.50	1.63	0.42	-0.73	0.989	+295.25
P1	n.	QG	5.30	2.13	0.28	-0.62	0.270	+148.59
P1	n.	QG	5.80	2.13	0.28	-0.69	0.511	+229.29
P1	n.	QG	7.00	1.81	0.33	-0.59	0.156	+77.31
P1	sap.	QK	8.00	2.09	0.28	-0.67	0.161	75.72
P1	sap.	Q	8.50	1.86	0.34	-0.58	0.100	+51.99
D2	s.c.	QK	1.30	1.82	0.33	-0.83	0.180	+37.31
D2	n.	QG	1.65	1.81	0.36	-0.86	0.250	+43.72
D2	sap.	QK	3.03	1.68	0.40	-0.81	0.080	+16.24
D2	sap.	QK	3.46	1.80	0.35	-0.83	0.001	-0.79
D2	sap.	Q-M	4.94	1.51	0.46	-0.75	0.060	+14.21
D2	sap.	QK	13.42	1.58	0.42	+1.04	0.001	+1.21
D2	sap.	QK	17.75	1.51	0.43	+0.13	0.001	+0.17
D2	sap.	QK	22.08	1.57	0.41	-0.07	0.001	0.000
D2	sap.	QK	26.85	1.56	0.40	-0.07	0.001	-0.01
D2	sap.	QK	30.74	1.52	0.44	-0.12	0.001	-0.08
D2	sap.	QK	35.00	1.60	0.40	+0.05	0.001	+0.15
D2	p.	QK	48.50	1.46	0.44	+0.00	0.001	0
D5	s.c.	QK	0.48	1.60	0.40	-0.49	0.550	+304.42
D5	s.c.	QK	2.16	1.51	0.43	-0.46	0.600	+333.84
D5	s.c.	QK	4.00	1.54	0.39	-0.46	0.650	+369.23
D5	s.c.	QK	5.63	1.58	0.40	-0.42	0.570	+357.49
D5	n.	QG	6.60	1.63	0.39	-0.77	0.405	+101.55
D5	n.	QG	7.36	1.68	0.36	-0.36	0.450	+328.81
D5	n.	QG	7.53	1.70	0.38	-0.81	0.365	+79.93
D5	n.	QG	8.00	2.20	0.28	-0.80	0.385	+113.65
D5	sap.	QK	10.82	1.68	0.37	-0.63	0.210	+88.77
D5	sap.	QK	12.04	1.55	0.45	-0.67	0.315	+109.41
D5	sap.	Q-G	12.82	1.60	0.48	-0.32	0.145	+106.41
D5	sap.	Q-G	16.70	1.68	0.42	-0.72	0.200	+63.35

P = pit; D = diamond drill hole; s.c. = sandy-clayey; n. = nodular; sap. = saprolite; p. = parent rock; Q = quartz; K = kaolinite; G = goethite; M = mica; ρ = bulk density; ϕ = porosity; $\epsilon_{Zr,w}$ = volumetric change; $\tau_{Au,w}$ = transport function.

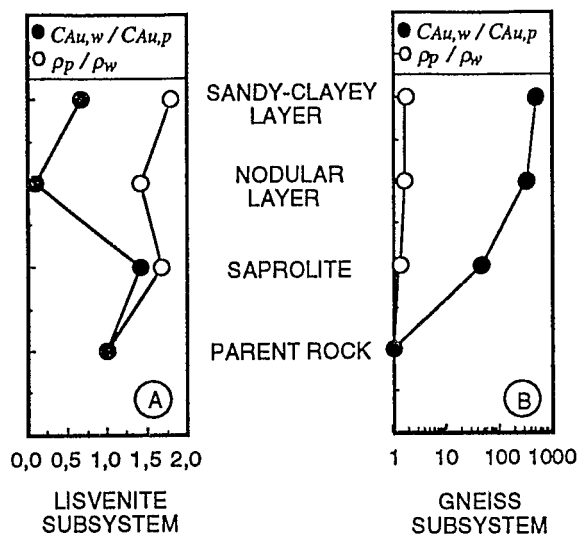


Fig. 3. Gold enrichment factor ($C_{Au,w}/C_{Au,p}$) and residual enrichment (ρ_p/ρ_w) profiles. (A) For the lisvenite sub-system. (B) For the gneiss sub-system.

layer. The Dondo Mobi weathering systems behaves globally as a collapsed system. Any variation in the transport function is limited by collapse and variation in the field is restricted by the volumetric change values of 0^- and -1 .

$R_{w/p}$ takes the value of unity in a given weathering system when the decrease in the bulk density in relation to the parent rock is exactly compensated by an increase in the concentration of the mobile element (Au in our study). Then the ratio $c_{Au,w}/c_{Au,p}$ is equal to ρ_p/ρ_w , which defines the upper value of residual enrichment, the lower value being 1.

If, in the lisvenite-derived weathering layers, the average $c_{Au,w}/c_{Au,p}$ is less than the corresponding ρ_p/ρ_w (Fig. 3A), then $R_{w/p} < 1$ and $\epsilon_{Zr,w} < 0$. We see immediately in Fig. 2 that $\tau_{Au,w}$ variation field ranges from 0^- to -1 . Gold leaves this sub-system during weathering.

In both gneiss and schist weathering layers containing gold ($Au > 0.001$ ppm), $c_{Au,w}/c_{Au,p}$ is > 2 , which is the maximum value obtained for ρ_p/ρ_w , so $R_{w/p} > 1$, while $\epsilon_{Zr,w} < 0$. The variation field of $\tau_{Au,w}$ (Fig. 2) depends upon the value of $\epsilon'_{Zr,w} = (1/R'_{w/p}) - 1$. For this value, $\tau_{Au,w} = 0$. Negative $\tau_{Au,w}$ values, with $\epsilon_{Zr,w} < \epsilon'_{Zr,w}$, would indicate enrichment, due to collapse, and then internal processes without any external input.

Note that, in Fig. 2, a symmetrical value, $\epsilon''_{Zr,w} = (1/R''_{w/p}) - 1$, corresponding to $\tau_{Au,w} = 0$, exists for dilational systems ($\epsilon_{Zr,w} > 0$), over which the decrease in concentration of element j would be strictly attributable to dilation. Our results (Tables 2 and 3) show that for any auriferous layers:

$$\frac{\rho_w c_{Au,w}}{\rho_p c_{Au,p}} \gg \frac{1}{\epsilon_{Zr,w} + 1}$$

For example, the calculation for the gibbsitic saprolite inherited from Archean gneiss (Table 2) which has the lowest detected gold content (0.019 ppm) of this sub-system gives:

$$R_{w/p} = \frac{1.74}{2.66} \times \frac{0.019}{0.001} = 12.43$$

$$\gg \frac{1}{\epsilon_{Zr,w} + 1} = \frac{1}{-0.26 + 1} = 1.35$$

$\tau_{Au,w}$ is then clearly greater than zero for any auriferous layer in the Archean gneiss and Proterozoic schist sub-systems (Fig. 2) and value of $\tau_{Au,w}$ is far beyond residual enrichment, as is shown, for example, in Fig. 3B for the gneiss sub-system. In addition, values of $\tau_{Au,w}$ increase upwards to the surface. We conclude that all the gold has been introduced from a surficial external source during weathering.

3.3 Overall mass transfer of gold during weathering within sub-systems

Solving eq. (2) for $m_{Au,w}$ gives eq. (5) for each sample:

$$m_{Au,w} = c_{Au,p} \rho_p v_p \tau_{Au,w} \quad (5)$$

with $[g] = [g][t]^{-1}[t][m]^{-3}[m]^3$ as dimensional equation.

The calculated mass of gold refers to the individual volume sample, v_p , and indicates the amount of gold transferred during the time of weathering.

To calculate the total mass of gold transferred through a weathering sub-system, the mass transport function may be integrated as a function of z , y and x , which are the depth and the lateral extensions of the auriferous sub-systems, respectively. The total mass of gold for a given weathering sub-system WS_n is given in theory by:

$$M_{Au,WS_n} = C_{Au,p} \rho_p \int_z \int_y \int_x \tau_{Au,w}(z,y,x) dz dy dx \quad (6)$$

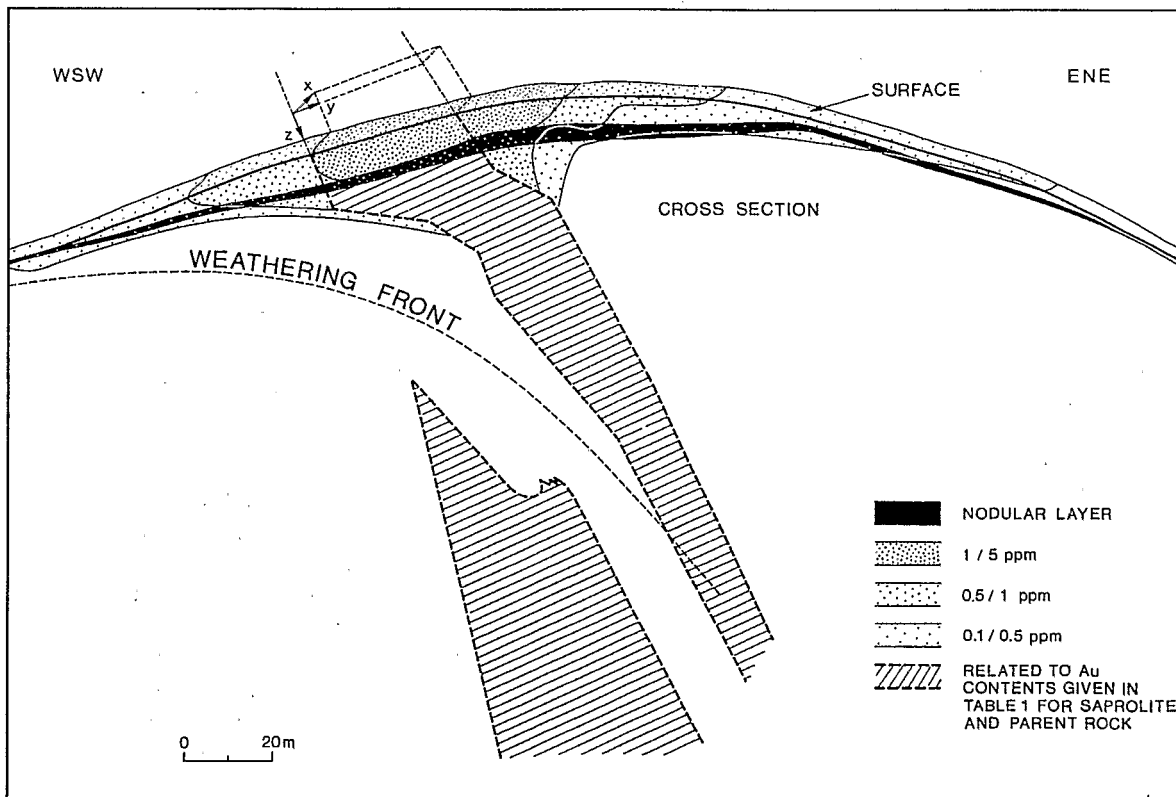


Fig. 4. Cross section showing the gold distribution and the geometric parameters used in overall gold mass transfer calculation.

TABLE 4

Total transferred gold mass $M_{Au,ws}$ and gold transfer density $T_{Au,ws}$ for weathering layers, L , of the three subsystems

subsystem (n)	layer (L)	$M_{Au,wsL}$ (g)	$T_{Au,wsL}$ (g/m ³)
lisvenite (1)	sandy-clayey	-2185.43	-10.960
	nodular	-1490.00	-11.920
	saprolite	-20156.50	-8.860
	parent rock	0.00	0.000
gneiss (2)	sandy-clayey	+155.49	+0.777
	nodular	+37.52	+0.600
	saprolite	+189.87	+0.584
	parent rock	0.00	0.000
schist (3)	sandy-clayey	+333.85	+0.763
	nodular	+88.53	+0.236
	saprolite	+158.18	+0.451
	parent rock	0.00	0.000

The total mass calculation, however, for a weathering sub-system WS_n can be approached by summation over each layer (L) of the sub-system as given by:

$$M_{Au,WS_n} = C_{Au,p} \rho_p \sum^L \tau_{Au,wL} V_{wL} \quad (7)$$

This has been produced by taking into consideration gold concentration of pits, drill core holes and auger holes samples (which define 5–1, 1–0.5 and 0.5–0.1 g/t haloes within the surficial part of the whole weathering mantle), and gold concentrations of drill core holes and pit hole samples for the auriferous lisvenite saprolite, in order to evaluate the mass of gold transfer within volumes defined by the ENE–WSW cross-sectional area (Fig. 4) and assuming a perpendicular lateral extent (x) of 1 m. The results of total mass transfers of gold (g) are given in Table 4 with the corresponding density of transfer T_{Au,WS_L} (g/m^3) ($= M_{Au,WS_L} / V_{WS_L}$) for each layer of the three sub-systems. This allows us to write:

$$\begin{aligned} M_{Au,WS_{lisvenite}} &= -23831 \text{ g} \\ M_{Au,WS_{gneiss}} &= +383 \text{ g} \\ M_{Au,WS_{schist}} &= +581 \text{ g} \end{aligned}$$

4. Physical and chemical behaviour of gold involved in supergene dispersion halo formation

Visible gold extracted from layers derived from gneiss and schist has been identified as mature

residual gold particles inherited from the lisvenite sub-system [11], which is clearly the external source of the dispersed gold. To evaluate the importance of mechanical processes in controlling the distribution of total gold within the halo, values of $\tau_{Au,w}$ are reported as function of distance from the auriferous lisvenite soil surface in Fig. 5. This distance has been calculated by addition of sample depth (z) to the lateral distance, d , which separates the lisvenite formation limit from the projection at the surface of the sample location. For each pit, d is identical for the whole set of samples.

The results stress that net gold mass gain declines linearly with the increasing distance from the lisvenite soil, laterally within layers and vertically downwards through layers of both gneiss and schist. Since no supergene gold has been identified and because the distribution is then independent of a potential geochemical barrier such as a weathering front redox change, we conclude that all the gold has been physically translocated during weathering. It has moved from the gold source towards the sandy-clayey layers and then downwards through nodular layers and saprolites. Important gold gains within sandy-clayey layers are positively correlated with the high porosity values (40% on average) of the quartz-kaolinite-rich matrix (Tables 2 and 3). It is clear that the source of the translocated gold corresponding to $M_{Au,WS_{gneiss}} = +383 \text{ g}$ and

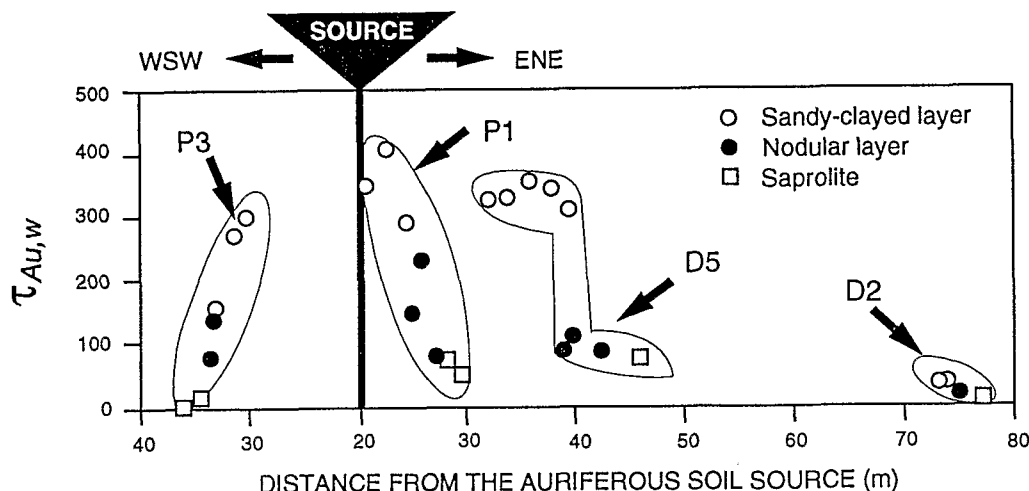


Fig. 5. Gold mass transport functions $\tau_{Au,w}$ within gneiss and schist sub-systems (P = pit, D = diamond drill hole) versus distance from the source.

$M_{Au,WS_{schist}} = +581$ g ($\Sigma = 964$ g) is not the extant lisvenite sandy-clayey layer but, rather, was the earlier degraded lisvenite regolith. Moreover, Colin and Vieillard [11] have demonstrated that gold particles extracted from the layers of the three sub-systems are subjected to increasing weathering upwards through the sub-system lisvenite, from the protore to the surface, and at the surface, laterally within both the gneiss and schist. Weathering continues downwards into the nodular layer derived from the schist and gneiss and saprolite. Dissolution pits, chemical roundness, a decrease in particle size and a decrease in the Ag content are the main features of particle weathering patterns.

We conclude that some gold was also lost by dissolution during translocation processes. Such dissolution probably took place within a layer similar to the present sandy-clayey layer. In addition, petrological and mineralogical relationships have demonstrated that the lisvenite sandy-clayey layer is mainly derived from a weathering layer close to the presently observable lisvenite saprolite. This means that the percentage of loss can be approached by calculation of the difference between the $T_{Au,WS_{lsc}}$ for the lisvenite sandy-clayey layer and the $T_{Au,WS_{ls}}$ for the lisvenite saprolite, divided by $T_{Au,WS_{lsc}}$ for the lisvenite sandy-clayey layer, which gives:

$$\frac{T_{Au,WS_{lsc}} - T_{Au,WS_{ls}}}{T_{Au,WS_{lsc}}} = \frac{-10.96 - (-8.86)}{-10.96} \quad (8)$$

The result (close to 20%) is hence the rate of gold dissolution under sandy-clayey layer conditions.

Thus, we can calculate the total amount of gold $\bar{M}_{Au,WS}$ initially mechanically imported within gneiss and schist sub-systems, which is simply obtained by:

$$\bar{M}_{Au,WS} + \frac{M_{Au,WS_{gneiss}} + M_{Au,WS_{schist}}}{1 - 0.19} \quad (9)$$

which gives $\bar{M}_{Au,WS} \approx 1200$ g. The volume of lisvenite sandy-clayey layer, V_{Lsc} (m^3), which has provided the total amount of gold $\bar{M}_{Au,WS}$ is given by eq. (10), where $C_{Au,Lsc}$ is the averaging gold concentration in the lisvenite sandy-clayey layer (g/t) and ρ_{Lsc} the average bulk density (t/m^3):

$$V_{Lsc} = \{\bar{M}_{Au,WS}\} / \{C_{Au,Lsc} \rho_{Lsc}\} \quad (10)$$

which gives $V_{Lsc} = 270$ m^3 . By knowing the present geometry of the lisvenite sandy-clayey body (Fig. 4) ($x = 1$ m, $y = 30$ m), the thickness (z , in meters) of the eroded sandy-clayey layer which has supplied gold is estimated at 9 m. The erosion rates of tropical soils developed on tectonically stable cratons approximate to $1-2$ $m/10^5$ yr in South American shields [33], 0.74 m in the Congo basin [34] and 1.05 m, on average, in West African shields [35]. Hence, we conclude that the gold dispersion halo of Dondo Mobi took shape over a period of about 0.86–1.22 million years.

The climatic conditions believed to have existed during the Quaternary are humid equatorial conditions [36]. In corroboration of this, the time taken for gold dispersion in our open weathering system can be calculated by assuming that the present physical and chemical environment has remained the same for the last million years.

As demonstrated in this work, by the strong negative values obtained for the gold transport function in the lisvenite saprolite (Table 1), and shown by the dissolution features of gold particles [11], dissolution is strongly involved in the dynamics of gold under equatorial rainforest conditions. Simultaneously, but also prior to mechanical transport, gold is affected by dissolution, which can be considered to be the first impetus of the dispersion processes. This implies that a thermodynamic approach to the solubility of gold is not only appropriate to supergene environment at Dondo Mobi but is also essential in understanding gold mobility.

5. Thermodynamic approach of gold geochemistry.

5.1 Determination of the supergene environment conditions at Dondo Mobi

According to rainfall studies in equatorial African forests [25], chloride and humic substances are feasible ligands for complexing Au. In constructing solubility diagrams for silver-bearing gold, measurements and estimates must be made for free chloride molality, humic substance concentrations, ionic strength, O_2 fugacity and pH. Chloride concentrations observed in the various spring waters around the deposit range from 10^{-5} to $10^{-3.8}$ mol/l. The minimum concentrations of

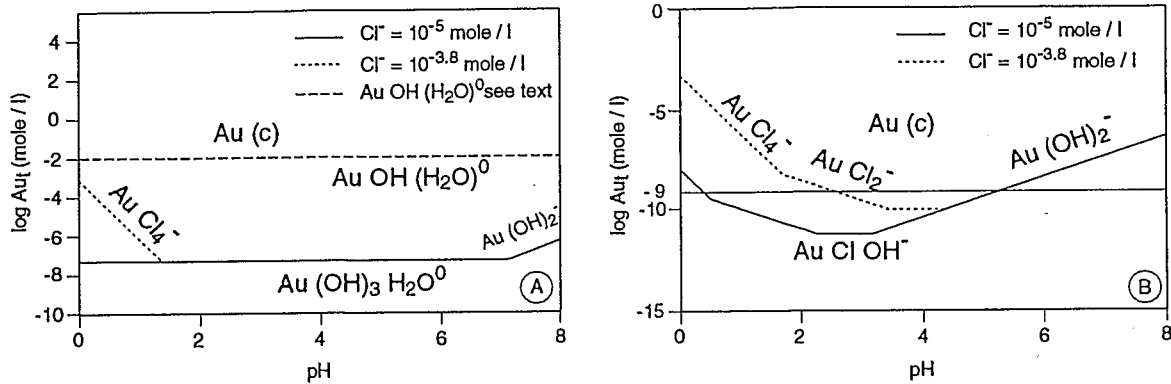


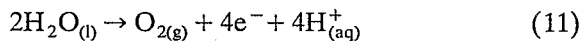
Fig. 6. Solubility of pure gold versus pH at different Cl^- molalities ($\text{Cl}^- = 10^{-3.8}$ and 10^{-5} mol/l) and $f_{\text{O}_2} = 10^{-0.68}$. (A) Calculated from [38]. (B) Calculated from [39]. Dotted line = $\text{Au}(\text{OH})\text{H}_2\text{O}^0$ complex.

soluble humic substances have been estimated at 5 mg/l in relation to average values in different Amazonian surface waters [26]. This value, however, can reach up to 50 mg/l according to [37]. As the ionic strength calculated for the spring water is very low, activity coefficients are close to unity and molalities approximate activities. The soil and water pH measurements range from 4 to 6.

For two sets of internal thermochemical data [38,39], the solubility of pure gold versus pH are given graphically (Fig. 6). Using an average total soluble gold concentration equal to 10^{-9} mol/l (100 ppt), the solubilization of pure gold in low chloride ($\text{Cl}^- = 10^{-5}$ mol/l) and high chloride ($\text{Cl}^- = 10^{-3.8}$ mol/l) conditions yields different results. With the Naumov's data set, the major species is $\text{Au}(\text{OH})_3\text{H}_2\text{O}^0$ which is stable for a broad range of pH (Fig. 6A). In this case, the gold metal fully dissolves for the corresponding gold value of 10^{-9} mol/l. Chloride ligands are only involved in gold complexing in the present case, which has a high chloride content, when the pH is very low.

Using the solubility of the complex $\text{Au}(\text{OH})\text{H}_2\text{O}^0$ found by experiment [40] would indicate (Fig. 6A) that the gold metal has a very high, unrealistic, solubility: $\text{Au}_t = 10^{-1.9}$ mol/l. These experimental results, in fact, are not very convincing because of the strong discrepancies between measured and calculated pH [40], because the gold concentrations are often different in both undersaturated and supersaturated solution procedures with a uncontrolled reversibility.

In addition, it seems inconceivable that, using the same data [40], the equilibrium between water and air or pure oxygen gas yields a pK close to 50 instead of 83, which is the recommended value for eq. (11):



In the N.B.S. thermochemical data set [39], the species $\text{Au}(\text{OH})_3\text{H}_2\text{O}^0$ is more unstable than other complexes of gold chloride. The main gold aqueous species (with increasing pH) are, successively: AuCl_4^- , AuCl_2^- , $\text{AuCl}(\text{OH})^-$ and $\text{Au}(\text{OH})_2^-$, as shown in Fig. 6B. The pH of solubilization of pure gold in solutions with a low and a high chloride concentration (for a value of $\text{Au}_t = 10^{-9}$ mol/l) are $\text{pH} = 0.5$ and $\text{pH} = 3$, respectively. These two very low pH values cannot explain the

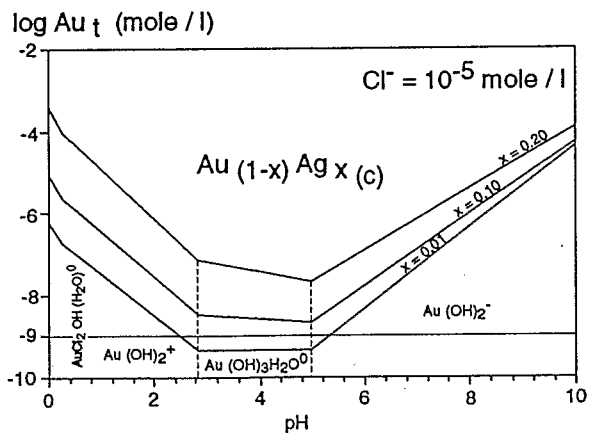


Fig. 7. Solubility of silver-bearing gold versus pH at a Cl^- molality equal to 10^{-5} mol/l and oxygen fugacity equal to $10^{-0.68}$, humic substances < 0.2 mg/l, $\text{Ag}_t = 10^{-8}$ mol/l.

TABLE 5

Gibbs free energies of formation for aqueous gold, silver complexes and other species

aqueous	species	Gibbs free energy of formation (kJ/mole)	foot note
Au ³⁺	Au(H ₂ O) ₄ ³⁺ (aq)	-515.40	(1)
	AuCl ₄ ⁻ (aq)	-240.68	(2)
	AuCl ₃ (H ₂ O) ^o (aq)	-314.49	(3)
	AuCl ₃ OH ⁻ (aq)	-309.85	(3)
	AuCl ₂ OH(H ₂ O) ^o (aq)	-401.82	(4)
	AuCl ₂ (OH) ₂ ⁻ (aq)	-375.83	(5)
	AuCl(OH) ₃ ⁻ (aq)	-435.81	(6)
	Au(OH) ₂ ⁺ (aq)	-83.69	(7)
	Au(OH) ₃ (H ₂ O) ^o (aq)	-542.14	(8)
	Au(OH) ₄ ⁻ (aq)	-486.97	(9)
Au ⁺	Au(H ₂ O) ₂ ⁺ (aq)	-310.83	(10)
	AuCl ₂ ⁻ (aq)	-151.17	(9)
	AuOHCl ⁻ (aq)	-215.23	(11)
	AuOH(H ₂ O) ^o (aq)	-286.20	(2)
	Au(OH) ₂ ⁻ (aq)	-345.60	(12,13)
Ag ⁺	Au(OH) ₂ ⁻ (aq)	-275.00	(12,13)
	Ag ⁺ (aq)	+77.1	(14)
	AgCl ₂ ⁻ (aq)	-215.4	(14)
Other species	AgCl ^o (aq)	-72.8	(14)
	H ₂ O(l)	-237.19	(15)
	Cl ⁻ (aq)	-131.29	(15)
	OH ⁻ (aq)	-157.336	(15)

(1) Calculated from the reaction: $\text{Au}(\text{H}_2\text{O})_4^{3+} + 2\text{e}^- \rightarrow \text{Au}(\text{H}_2\text{O})_2^+ + 2\text{H}_2\text{O}(\text{l})$ $E^\circ = 1.4 \text{ V}$ [41].

(2) [G. Koroleva, pers. commun., 1988].

(3) Calculated from the reactions: $\text{AuCl}_4^-(\text{aq}) + \text{H}_2\text{O}(\text{l}) \rightarrow \text{AuCl}_3(\text{H}_2\text{O})^\circ(\text{aq}) + \text{Cl}^-(\text{aq})$; $\log K = -5.4$; and $\text{AuCl}_3(\text{H}_2\text{O})^\circ(\text{aq}) \rightarrow \text{AuCl}_3\text{OH}^-(\text{aq}) + \text{H}^+(\text{aq})$; $\log K = -0.59$ [42].(4) Calculated from the reaction: $\text{AuCl}_3\text{OH}^-(\text{aq}) + \text{H}_2\text{O}(\text{l}) \rightarrow \text{AuCl}_2\text{OH}(\text{H}_2\text{O})^\circ(\text{aq}) + \text{Cl}^-(\text{aq})$; $\log K = -2.44$ [42].(5) Calculated from the reaction: $\text{AuCl}_2\text{OH}(\text{H}_2\text{O})^\circ(\text{aq}) \rightarrow \text{AuCl}_2(\text{OH})_2^-(\text{aq}) + \text{H}^+(\text{aq})$; $\log K = -4.55$ [42].(6) Calculated from the reaction: $\text{AuCl}_2(\text{OH})_2^-(\text{aq}) + \text{H}_2\text{O}(\text{l}) \rightarrow \text{AuCl}(\text{OH})_3^-(\text{aq}) + \text{Cl}^-(\text{aq}) + \text{H}^+(\text{aq})$; $\log K = -8.05$ [42].(7) Calculated from the reaction: $\text{Au}(\text{OH})_3(\text{c}) \rightarrow \text{Au}(\text{OH})_2^+(\text{aq}) + \text{OH}^-(\text{aq})$; $\log K = -11.2$ [44].(8) Calculated from the reaction: $\text{Au}(\text{OH})_3(\text{c}) + \text{H}_2\text{O}(\text{l}) \rightarrow \text{Au}(\text{OH})_3(\text{H}_2\text{O})^\circ(\text{aq})$; $\log K = -7.7$ [44] with $\Delta G^\circ_f \text{ Au}(\text{OH})_3(\text{c}) = -348.9 \text{ kJ/mole}$ [38].(9) [38]. (10) [45]. (11) Calculated from the reaction: $\text{AuCl}_2^-(\text{aq}) + \text{OH}^-(\text{aq}) \rightarrow \text{AuOHCl}^-(\text{aq}) + \text{Cl}^-(\text{aq})$; $\log K = 6.66$ [46]. (12) [40]. (13) See text. (14) [39]. (15) [47].

solubilization of gold by the chloride ion because the lowest pH measured in the spring waters and in soil waters is 4. However, for pH values over 5.3, gold should dissolve and the gold species present should be $\text{Au}(\text{OH})_2^-$.

In the following section, the gold solubility diagrams versus pH are used for pure gold and for silver and gold alloys, whose thermodynamic mixing functions are known.

5.2 Setting of stability diagrams

Table 5 lists the Gibbs free energies of formation of aqueous species and complexes of gold and silver. The thermodynamic value of $\text{AuOH}(\text{H}_2\text{O})^\circ$ given by [40] is not used in this work. Table 6 lists the Gibbs free energies of formation of crystalline compounds of gold and silver involved in our study. The silver content

ranks from 0 to 20%, as demonstrated by 1530 microprobe analyses of gold particles [11]. From these two tables, the solubility of any silver-bearing gold (stoichiometric formula $Au_{(1-x)}Ag_x$) in water with or without Cl^- can be expressed by $(1-x) \log(Au)_t + x \log(Ag)_t$ versus pH.

In order to express the total molality of gold versus pH, the total molality of silver has to be constant. The very high molality of free chloride ion ($Cl^- = 10^{-3.8}$ mol/l) and the absence of chloroargyrite ($AgCl$) in the weathering system (chloroargyrite is a very insoluble mineral) together determine the value of $\log [Ag^+]$ using:

$$\log [Ag^+] + \log [Cl^-] = -9.74 \quad (12)$$

The maximum value of the total silver molality is $10^{-5.94}$ mol/l. In this range of chloride molality the major ion is Ag^+ and the other aqueous chloride silver complexes, such as $AgCl^0$ and $AgCl_2^-$, are negligible. Hence, we choose arbitrarily a value of total silver molality equal to 10^{-8} mol/l (1.08 ppb). It should be kept in mind that a lowering of one unity of total molality of silver leads to a lifting of $x/1-x$ moles of the total molality of gold, and the reverse is also true.

Figure 7 shows the theoretical solubility of silver-bearing gold in a natural surficial environment in low chloride and low humic substances conditions ($Cl^- = 10^{-5}$ mol/l and $HS < 0.2$ mg/l), with $f_{O_2} = 10^{-0.68}$. The solubility of silver-bearing gold gives different gold species with increasing pH: $AuCl_2OH(H_2O)^0$ from pH 0 to 0.4, $Au(OH)_2^+$ between pH 0.4 and 2.7,

$Au(OH)_3(H_2O)^0$ from 2.7 to 5.0 and $Au(OH)_2^-$ for pH values higher than 5.0. The stability constants of the aqueous species $Au(OH)_2^-$, measured by [43,46] must be used with caution. This value is, in fact, too high, but the correction factor is unknown. Gold which has a high silver content ($x > 0.2$) is very unstable and fully dissolves in natural surficial systems. In very low oxygen fugacity conditions, which occur, for example, in weakly porous media, the stability of silver-bearing gold may increase.

5.3 Influence of chloride ion on stability diagrams

Figure 8 shows the solubility of silver-bearing gold $Ag_xAu_{(1-x)}$ calculated for the maximum value of $Cl^- = 10^{-3.8}$ mol/l found in the spring waters. The solubility of electrum involves two new aqueous chloride species in the comparison of results obtained for $Cl^- = 10^{-5}$ mol/l (Fig. 7): $AuCl_4^-$ in pH range 0-0.8 and $AuCl_2^-$ in pH range 2.5-2.7. $AuClOH^-$ appears only when $Cl^- > 10^{-3.5}$ mol/l and becomes more stable than $Au(OH)_3(H_2O)^0$. The other chloride gold complexes (given in Table 5) appear only for higher Cl^- values, so they are not involved in this diagram. The results stress that pure gold remains insoluble in solutions having $Cl^- = 10^{-5}$ mol/l, as well as in solutions having $Cl^- = 10^{-3.8}$ mol/l, for a value of $Au_t = 10^{-9.3}$ mol/l, which is the average value of the gold content in natural waters around gold deposits [21].

TABLE 6

Gibbs free energies of formation for minerals involved in the (Au, Ag) system

minerals	Gibbs free energy of formation (kJ/mole)	foot note
Au(c)	0	(1)
Ag(c)	0	(2)
AgCl(c)	-109.789	(1),(3)
Au _{0.99} Ag _{0.01}	-0.29	(4)
Au _{0.9} Ag _{0.1}	-2.21	(4)
Au _{0.8} Ag _{0.2}	-3.78	(4)

(1) [39]. (2) [47]. (3) [38]. (4) Calculated from experimental studies [48] measured at 800°K and extrapolated to 298.15°K by the following relationships for the alloys $Au_{(1-x)}Ag_x$ (in J/mol): $\Delta H_{mix} = -[20292 - 3347(1-x)] x(1-x)$; $\Delta S_{excess} = -5.75x(1-x)$; $\Delta G_{mix} = \Delta H_{mix} - T(\Delta S_{ideal} + \Delta S_{excess})$. This calculation was made by assuming the total independence between temperature and enthalpy and excess entropy of mixing.

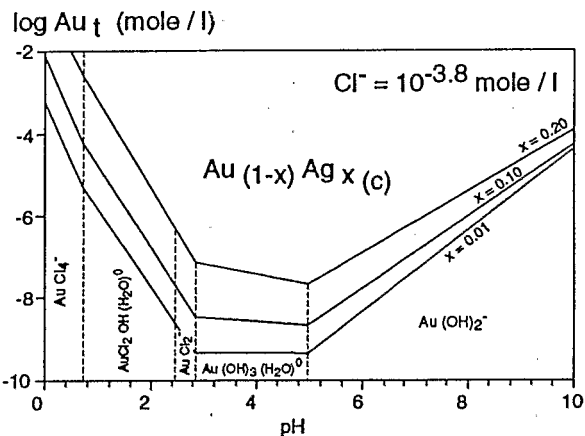
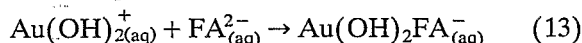


Fig. 8. Solubility of silver-bearing gold versus pH at a Cl^- molality equal to $10^{-3.8}$ mol/l and oxygen fugacity equal to $10^{-0.68}$, humic substances < 0.2 mg/l, $\text{Ag}_t = 10^{-8}$ mol/l.

5.4 Influence of organic matter in the stability of gold bearing minor silver

The only available dissociation constant for gold with organic matter is from [44]. Chateau and co-workers measured the stability constant of $\text{Au}(\text{OH})_2^+$ with fulvic acid (FA) in the proportion 1:1. The equation of dissociation of gold fulvic acid complex is:



The stability constants were measured at pH 3.5, 5.8 and 7.5, and are $\log b = 2.7 \times 10^6$, 5.6×10^8 and 8.9×10^9 , respectively. The dissociation constants for the carbonyl groups in the fulvic

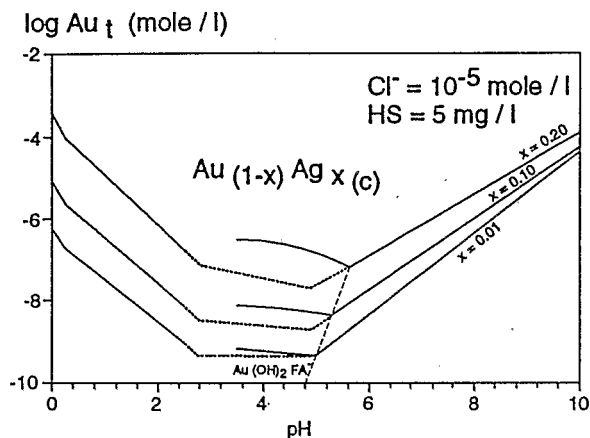


Fig. 9. Solubility of silver-bearing gold versus pH at a Cl^- molality equal to 10^{-5} mol/l, oxygen fugacity equal to $10^{-0.68}$, humic substances equal to 5 mg/l, $\text{Ag}_t = 10^{-8}$ mol/l. Dotted line = the limit of solubility without organic matter.

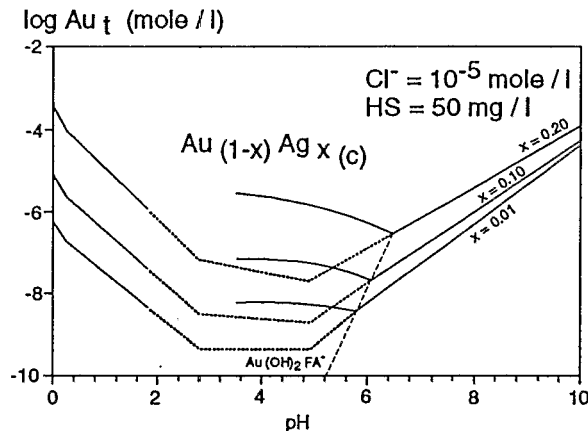


Fig. 10. Solubility of silver-bearing gold versus pH at a Cl^- molality equal to 10^{-5} mol/l, oxygen fugacity equal to $10^{-0.68}$, humic substances equal to 50 mg/l, $\text{Ag}_t = 10^{-8}$ mol/l. Dotted line = the limit of solubility without organic matter.

acid are $K_1 = 2.10^{-3}$ and $K_2 = 5.10^{-5}$ [44]. The weighted mean molecular masses of fulvic acid were determined from the linear pH dependence and are 326 at pH 3.5, 3400 at pH 5.8 and 5600 at pH 7.5.

Since fulvic acid is the main component of humic substances (HS) in tropical surficial systems [26], it is possible to use these constants to study the stability of gold in relation to organic activity. Calculations have been made with $\text{HS} = 5$ mg/l (Fig. 9), which is the average concentration in tropical surficial systems [26], and $\text{HS} = 50$ mg/l (Fig. 10), which characterizes tropical soils with intense microbial activity [37]. The trend towards a higher solubility of Au with increasing Ag contents is also demonstrated for fulvic acid: not only is the HS concentration higher but the possibility that organo-metallic complexes form instead of inorganic ones is greater, which makes it easier for pure gold to dissolve. In conditions of high humic substances, nearly pure Au is soluble over a broader pH range (3.5–6). We conclude that organic matter could play a major role in gold complexation in surficial acidic conditions at Dondo Mobi.

6. Conclusions

The physical and chemical mobility of gold throughout the global weathering system of Dondo Mobi has been quantitatively addressed by calculating the gold mass transfer during weather-

ing and by proposing a thermodynamic approach to gold solubility under equatorial rainforest conditions.

While weathering progresses, an increasing amount of gold-rich rocks are being digested, and gold has been both physically and chemically affected. Gold particles have transferred from the lisvenite-derived soil towards the formerly barren Archean gneiss and the formation derived from Proterozoic schist to form a 200 m wide supergene gold dispersion halo, which extends beyond the auriferous body. The high specific gravity of gold makes translocations down through the highly porous surficial sandy-clayey and nodular layers within the root zone very easy. Within the halo, from the surface soil towards the saprolite, the gradient of decreasing values for gold mass importation, and the absence of supergene gold, stress that gold distribution is linked to mechanical barriers and not to geochemical barriers.

We have demonstrated that the physical movement (from the source towards gneiss and schist formations, within a volume defined by the cross-sectional area of the weathering systems and a thickness of 1 m) of a mass of around 1.2 kg of gold has taken place during weathering and have calculated that the supergene dispersion halo took shape over about 0.86–1.22 million years, assuming that the present physical and chemical equatorial humid environment remained the same during that time.

At the scale of the entire weathering system at Dondo Mobi, gold is easily released because of strong dissolutional processes which operate before and during physical translocation. Transport mass function results demonstrate that the total balance of gold transfer is negative, while the net mass gain in gold calculated for Archean gneiss and Proterozoic schist does not compensate the net mass of gold lost from the auriferous lisvenite. We conclude that, opposite to what is generally believed, lateritic physical and chemical processes do not generate gold enrichment, but rather induce a strong loss of gold under acidic equatorial rainforest conditions. At Dondo Mobi, marine-derived Cl-rich rain water and humic substances, resulting from intense biological activity, provide ligands capable of complexing Au.

Taking into account hydrolysis reactions, three main gold complexes are a function of corre-

sponding inorganic and organic ligand concentrations. These are $\text{Au}(\text{OH})_3(\text{H}_2\text{O})^\circ$, AuClOH^- and $\text{Au}(\text{OH})_2\text{FA}^-$. In addition, we have demonstrated that the solubility of gold increases with the Ag content and that pure gold only dissolves under organic activity conditions. These gold complexes are believed to be stable under surficial equatorial rainforest conditions. We propose that such complexes have left the Dondo Mobi weathering mantle and moved towards the river system in the course of both physical and chemical processes involved in the formation of the weathering system.

Gold mobility in an equatorial rainforest lateritic environment is controlled by both chemical and short-distance translocation processes, which take place during the evolution of long-term open weathering systems. These systems are the result of the combined interaction of rock, meteoric water and biological agents. The ubiquity of such interaction between lithosphere, hydrosphere, atmosphere and biosphere in surficial systems makes it possible to extend our results to most lateritic and surficial weathering systems. Nevertheless, further studies should take into account possible f_{O_2} changes in weathering soil solutions.

Acknowledgements

This work was made possible by the interest of the Gabonese Geological Survey and of the Joint Venture "Or-Eteke". Collaboration and dialogues with Daniel Nahon, Georges Brimhall, Marc Benedetti, Paulo Vasconcelos and Christopher Lewis are much appreciated. We thank Jean Jacques Motte and Raymond Dassule for their assistance with the artwork.

References

- 1 R.E. Smith, Current research at CSIRO Australia on multi-element laterite geochemistry for detecting concealed mineral deposits, *Chem. Geol.* 60, 205–211, 1987.
- 2 C.R.M. Butt, A basis for geochemical exploration models for tropical terrains, *Chem. Geol.* 60, 5–16, 1987.
- 3 P. Lecomte, Stone line profiles: Importance in geochemical exploration, *J. Geochem. Explor.* 30, 35–61, 1988.
- 4 R. Davy and M. El Ansary, Geochemical pattern in the laterite profile at the Boddington gold deposit, Western Australia, *J. Geochem. Explor.* 26, 119–124, 1986.
- 5 A.F. Wilson, The economic significance of non hydrothermal transport of gold, and the accretion of large gold

- nuggets in laterite and other weathering profiles in Australia, *Spec. Publ. Geol. Soc. Sci. Afr.* 7, 229–234, 1983.
- 6 A.W. Mann, Mobility of gold and silver in lateritic weathering profiles: Some observations from western Australia, *Econ. Geol.* 79, 38–49, 1984.
 - 7 P. Freyssinet, H. Zeegers and Y. Tardy, Morphology and geochemistry of gold grains in lateritic profiles of southern Mali, *J. Geochem. Explor.* 32, 17–31, 1989.
 - 8 D. Michel, Concentration of gold in in situ laterites from Mato Grosso, *Miner. Deposita* 22, 185–189, 1987.
 - 9 L.M. Lawrance, Behavior of gold within the weathering profile in the Yilgarn Block, Western Australia, *Publ. Univ. Western Australia* 12, 335–351, 1988.
 - 10 B. Grimm and G. Friedrich, Weathering effects on supergene gold in soils of a semiarid environment, Gento Do Ouro, Brazil, *Chem. Geol.* 84, 70–73, 1990.
 - 11 F. Colin and P. Vieillard, Behavior of gold in the lateritic equatorial environment: Weathering and surface dispersion of residual gold particles, at Dondo Mobi, Gabon, *Appl. Geochem.* 6, 279–290, 1991.
 - 12 P. Vasconcelos and J.R. Kyle, Gold geochemistry in a semi-arid weathering environment, *Econ. Geol.*, in press, 1992.
 - 13 K.B. Krauskopf, The solubility of gold, *Econ. Geol.* 46, 858–870, 1951.
 - 14 P.L. Cloke and W.C. Kelly, Solubility of gold under inorganic supergene conditions, *Econ. Geol.* 59, 259–270, 1964.
 - 15 L. Ong and V.E. Swanson, Natural organic acids in the transportation, deposition and concentration of gold, *Q. Colo. Sch. Mines* 64, 395–425, 1969.
 - 16 J. Pouradier and M.C. Gadet, Electrochimie des sels d'or, II Aurichlorure, *J. Chim. Phys.* 62, 1185, 1966.
 - 17 W.E. Baker, The role of humic acid in the transport of gold, *Geochim. Cosmochim. Acta* 42, 645–649, 1978.
 - 18 T. Seward, The transport and deposition of gold in hydrothermal systems, in: *Gold 82, The Geology, Geochemistry, and Genesis of Gold Deposits*, R.P. Foster, ed., pp. 165–181, Balkema, Rotterdam, 1984.
 - 19 J.G. Webster, The solubility of gold and silver in the system Au–Ag–S–O₂–H₂O at 25°C and 1 atm. *Geochim. Cosmochim. Acta* 50, 1837–1845, 1986.
 - 20 R. Stoffregen, Observation on the behavior of gold during supergene oxidation at Summitville, Colorado, U.S.A., and implications for electrom stability in the weathering environment, *Appl. Geochem.* 1, 549–558, 1986.
 - 21 M. Benedetti, Géochimie de l'or: Mécanismes de transport et de dépôt, *Sci. Géol. Mém.* 91, 1–148, 1991.
 - 22 C.F. Gleeson and R. Poulin, Gold exploration in Niger using soils and termitaria, *J. Geochem. Explor.* 331, 253–283, 1989.
 - 23 R.E. Smith and J.L. Perdrix, Pisolithic laterite geochemistry in the Golden Grove massive sulphide district, Western Australia, *J. Geochem. Explor.* 18, 131–164, 1983.
 - 24 D. Nahon, Introduction to the petrology of soils and chemical weathering, 313 pp., Wiley, New York, 1991.
 - 25 J.P. Lacaux, J. Servant, M.L. Huertas, R. Cros, R. Delmas and A. Andreae, Precipitation chemistry from remote sites in the African equatorial forest, *EOS Trans. Am. Geophys. Union* 69 (44), 1069, 1988.
 - 26 J.R. Ertel, J.I. Hedges, H. Devol, J.E. Richey and M.N.G. Ribeiro, Dissolved humic substances of the Amazon River system, *Limnol. Oceanogr.* 31, 739–754, 1986.
 - 27 J.B. Harrison, The catamorphism of igneous rock under humid tropical conditions, *Imp. Bur. Soil Sci., Harpenden*, 79 pp., 1933.
 - 28 N. Leneuf, L'altération des granites calco-alcalins et des granodiorite en Côte d'Ivoire forestière et les sols qui en sont dérivés, Thèse Fac. Sci., Paris, 210 pp., 1959.
 - 29 G. Millot and M. Bonifas, Transformations isovolumétriques dans les phénomènes de latérisation et de bauxitisation, *Bull. Serv. Carte Géol. Alsace Lorraine* 8, 3–10, 1955.
 - 30 G.H. Brimhall and W.E. Dietrich, Constitutive mass balance relations between chemical composition, volume, density, porosity, and strain in metasomatic hydrochemical systems: results on weathering and pedogenesis, *Geochim. Cosmochim. Acta* 51 (3), 567–587, 1986.
 - 31 F. Colin, G.H. Brimhall, D. Nahon, C.J. Lewis, A. Baronnet and K. Danty, Equatorial rain forest lateritic soils: A geomembrane filter, *Geology* 20, 523–526, 1992.
 - 32 D. Muller, G. Bocquier, D. Nahon and H. Paquet, Analyse des différenciations minéralogiques et structurales d'un sol ferrallitique à horizons nodulaires du Congo, Cah. ORSTOM, Sér. Pédologie 18 (2), 87–109, 1980.
 - 33 R.F. Stallard, Weathering and erosion in the humid tropics, in: *Physical and chemical weathering in geochemical cycles*, A. Lerman and M. Meybeck, eds., pp. 225–246, Kluwer, Dordrecht, The Netherlands, 1988.
 - 34 R.R. Nkounkou and J.L. Probst, Hydrology and geochemistry of the Congo river system, *Mitt. Geol. Paläontol. Inst. Univ. Hamburg* 44, 483–508, 1987.
 - 35 J.Y. Gac, Géochimie du bassin du lac Tchad. Bilan de l'altération, de l'érosion et de la sédimentation, *Trav. Doc. ORSTOM* 123, 251, 1980.
 - 36 B. Kobilsec, Géochimie et pétrographie des bauxites latéritiques d'Amazonie Brésilienne. Comparaison avec l'Afrique, l'Inde et l'Australie, Thèse Univ. Louis Pasteur, Strasbourg, 201 pp., 1990.
 - 37 P.A. Sanchez, D.E. Bandy, J.H. Villachica and J.J. Nicholaidis, Amazon basin soils: Management for continuous crop production, *Science* 21, 821–827, 1982.
 - 38 G.B. Naumov, B.N. Ryschenko and J.L. Khodakovsky, *Handbook of Thermodynamic Data*, 239 pp., Moscou Atomizdat, Moscow, 1971 (in Russian).
 - 39 D.D. Wagman, W.H. Evans, V.B. Parker, R.H. Schumm, I. Halow, M.S. Bailey, K.L. Churney and R.L. Nuttall, The NBS tables of chemical thermodynamic properties: selected values for inorganic and C1 and C2 organic substances in S.I. units, *J. Phys. Chem. Ref. Dat.* II (2), 1–392, 1982.
 - 40 D. Vlassopoulos and S.A. Wood, Gold speciation in natural waters. I—Solubility and hydrolysis reactions of gold in aqueous solution, *Geochim. Cosmochim. Acta* 54, 3–12, 1990.
 - 41 R. Puddephat, Gold, in: *Comprehensive Coordination Chemistry*, G. Wilkinson, ed., Vol. 5, pp. 861–923, Pergamon, Amsterdam, 1987.
 - 42 Ye.A. Nechaev and A. Zvonareva, Adsorption of chloride complexes of gold (III) on goethite, *Kolloid Zh.* 45 (5), 908–911, 1984.

- 43 H. Chateau, M.C. Gadet and J. Pouradier, *Electrochimie des sels d'or. I—Acide auro et aurichlorydrique et sels correspondants*, *J. Chim. Phys.* 62, 203-216, 1966.
- 44 G.M. Varshal, T.K. Velyukhanova and N.N. Baranova, *The geochemical role of gold (III) fulvate complexes*, *Geokhimiya* 3, 413-420, 1984.
- 45 P.R. Johnson, J.M. Pratt and R.I. Tilley, *Experimental determination of the standard reduction potential of the gold (I) ion*, *J. Chem. Soc. Chem. Commun.* ?, 606-607, 1978.
- 46 M.C. Gadet and J. Fouradier, *Hydrolyse des complexes de l'or I*, *C.R. Acad. Sci. Paris Sér. C* 275, 1061-1064, 1972.
- 47 Codata Task Group, *Recommended key values for thermodynamic*, 1977, *Codata Bull.* 28, 1-17, 1977.
- 48 R. Hultgren, P.D. Desai, D.T. Hawkins, M. Gleiser and K.K. Kelley, *Selected Values of the Thermodynamic Properties of Binary Alloys*, pp. 339-346, Am. Soc. Metals, Metals Park, Ohio, 1956.